Biophysical Journal
Article

Biophysical Society

A mechanism for slow rhythms in coordinated pancreatic islet activity

Nicole Bruce,[1] James Thornham,[2] I-An Wei,[3] Michael G. Roper,[2,3] and Richard Bertram[1,2,4,*]
[1]Department of Mathematics, Florida State University, Tallahassee, Florida; [2]Program in Molecular Biophysicis, Florida State University, Tallahassee, Florida; [3]Department of Chemistry and Biochemistry, Florida State University, Tallahassee, Florida; and [4]Program in Neuroscience, Florida State University, Tallahassee, Florida

ABSTRACT Insulin levels in the blood oscillate with a variety of periods, including rapid (5–10 min), ultradian (50–120 min), and circadian (24 h). Oscillations of insulin are beneficial for lowering blood glucose and disrupted rhythms are found in people with type 2 diabetes and their close relatives. These in vivo secretion dynamics imply that the oscillatory activity of individual islets of Langerhans are synchronized, although the mechanism for this is not known. One mechanism by which islets may synchronize is negative feedback of insulin on whole-body glucose levels. In previous work, we demonstrated that a negative feedback loop with a small time delay, to account for the time required for islets to be exposed to a new glucose concentration in vivo, results in small 3–6 islet populations synchronizing to produce fast closed-loop oscillations. However, these same islet populations could also produce slow closed-loop oscillations with periods longer than the natural islet oscillation periods. Here, we investigate the origin of the slow oscillations and the bistability with the fast oscillations using larger islet populations (20–50 islets). In contrast to what was observed earlier, larger islet populations mainly synchronize to longer-period oscillations that are approximately twice the delay time used in the feedback loop. A mean-field model was also used as a proxy for a large islet population to uncover the underlying mechanism for the slow rhythm. The heterogeneous intrinsic oscillation periods of the islets interferes with this rhythm mechanism when islet populations are small, and is similar to adding noise to the mean-field model. Thus, the effect of a time delay in the glucose feedback mechanism is similar to other examples of time-delayed systems in biology and may be a viable mechanism for ultradian oscillations.

SIGNIFICANCE Insulin oscillations are essential for proper glucose uptake but the mechanisms by which the numerous islets in a pancreas synchronize are not known. Here, we show computationally and experimentally that populations of islets can be synchronized to long-period oscillations using a delayed negative feedback loop of islet activity on extracellular glucose. The averaging over many islets reduces the variability due to heterogeneity in the individual islet periods, facilitating the establishment of long-period oscillations. The mechanism is a viable means to producing longer-period oscillations, such as ultradian oscillations, while other mechanisms may be responsible for different oscillation periods found in vivo.

INTRODUCTION

Insulin secretion is pulsatile, originating from β cells located within pancreatic islets of Langerhans. Pulsatile insulin secretion is necessary to effectively regulate blood sugar (1,2), and abnormal insulin pulsatility is observed in people with type 2 diabetes and their first-degree relatives (3,4). In single islets, pulsatile insulin secretion is driven by bursts of electrical impulses and accompanying oscillations in intracellular Ca^{2+} concentration (4–6). As this pulsatility is reflected in blood insulin measurements (7–10), the activity of hundreds of thousands of islets must be synchronized. Two mechanisms have been proposed for pancreatic islet synchronization (11). In one, islet activity is coordinated through neural impulses from pancreatic ganglia. The basis for this hypothesis is bursts of electrical activity in ganglion cells that occur every 6–8 min (12), similar to the observed ∼5 min period of insulin oscillations (7–9,11,13), and by preganglionic vagal neurons innervating the pancreas in close proximity to islets (14–16). By sending periodic stimuli to islets, the pancreatic ganglia may serve

Submitted April 18, 2024, and accepted for publication July 22, 2024.
*Correspondence: rbertram@fsu.edu
Nicole Bruce and James Thornham contributed equally to this work.
Editor: N.G. Cogan.
https://doi.org/10.1016/j.bpj.2024.07.028

as a pacemaker that coordinates their activity. In previous work, we tested the plausibility of this mechanism with computer simulations and in an in vitro setting, and found that both periodic and aperiodic forcing are sufficient to achieve synchronization (17). In the second mechanism, islet activity is hypothesized to be coordinated through a negative feedback loop between the pancreas and liver. Insulin secreted in response to a high blood glucose level causes a net uptake of glucose into the liver, lowering the glucose concentration in the blood. This reduction in blood glucose is felt by the entire islet population and acts as a global coordinating signal to synchronize islet activity (11,18). Recently, the negative feedback mechanism of synchronization was tested in both model islets and in vitro islets with the inclusion of a time delay of varying lengths in the negative feedback (19). This time delay was added to account for the time it takes for the effects of the glucose regulation by the liver to reach the islets through the circulation. Without a time delay in the negative feedback, islet populations synchronized to produce what we refer to as "fast closed-loop oscillations" with ∼5 min periods (19,20). With a time delay up to 7 min in the negative feedback, islet populations continued to synchronize to produce fast closed-loop oscillations, but also produced "slow closed-loop oscillations" in which the period increased with the time delay and was much longer than the natural islet period (19). In the latter case, islet oscillations were not synchronized, but instead were grouped into longer-period episodes. In addition, it was found that the system is bistable with regard to the fast and slow closed-loop oscillations, as one islet population was capable of generating both rhythms for a single time delay and could be perturbed from one rhythm to the other. In this report, we investigate the origin of the slow closed-loop oscillations, and the bistability with the fast closed-loop oscillations. This is done through a combination of mathematical modeling and in vitro experiments employing a newly developed microfluidic device. The modeling suggests that the slow oscillations are more prevalent with larger islet populations, and to test this prediction a new microfluidic platform was designed to allow us to increase the number of islets involved in the negative feedback.

MATERIALS AND METHODS

Chemicals and reagents

Sodium chloride (NaCl), calcium chloride ($CaCl_2$), magnesium chloride ($MgCl_2$), dimethyl sulfoxide (DMSO), and Fura 2 acetoxymethyl ester were acquired from Sigma-Aldrich (Saint Louis, MO). Potassium chloride (KCl) and tricine were from VWR International (Radnor, PA). Sodium hydroxide, glucose (dextrose), and bovine serum albumin were purchased from Fisher Scientific (Pittsburgh, PA). Fetal bovine serum, penicillin-streptomycin, gentamicin, and Pluronic F-127 were from Thermo Fisher Scientific (Waltham, MA). Collagenase P was from Roche Diagnostics (Indianapolis, IN). RPMI 1640 was from Corning (Corning, NY). Polydimethylsiloxane (PDMS) and curing agent were from Dow Corning (Midland, MI). SU-8 photoresist was from Kayaku Advanced Materials (Westborough, MA). All solutions were made with ultrapure deionized water (Millipore, Bedford, MA). Glucose solutions were prepared in a balanced salt solution (BSS) composed of 125 mM NaCl, 5.9 mM KCl, 2.4 mM $CaCl_2$, 1.2 mM $MgCl_2$, and 25 mM tricine [pH 7.4], with 1 mg mL^{-1} bovine serum albumin.

Isolation and culture of islets of Langerhans

The islet isolation protocol was approved by the Florida State University Animal Care and Use Committee (protocol no. TR202300000025). Islets of Langerhans were obtained from 25–40 g male CD-1 mice (Charles River Laboratories, Wilmington, MA) by collagenase P digestion as described previously (21,22). Isolated islets were incubated in RPMI 1640 medium with 11 mM glucose, L-glutamine, 10 fetal bovine serum, 100 U mL^{-1} penicillin, 100 μg mL^{-1} streptomycin, and 10 μg mL^{-1} gentamicin at 37°C and 5% CO_2. Islets were kept in the incubator and used within 4 days after isolation. Typically, islets were isolated from two mice and were not mixed during experiments.

Microfluidic device and $[Ca^{2+}]_i$ detection

The PDMS-glass hybrid microfluidic device is an evolution of a previously developed design (19), now incorporating four chambers (Fig. 1). The device was fabricated using conventional soft photolithography with SU-8 2050 photoresist. All channels were 250 × 50 μm (width × height). There were two inputs connected to reservoirs filled with BSS and high and low glucose, and flow was gravity driven with a constant total flow rate from the two inputs. The two reservoirs were suspended above the device and the heights of each were adjusted by a pulley system controlled by a LabVIEW program (National Instruments, Austin, TX), which changed the flow rates of the two inputs (23). The mixed buffer delivered to the islets was split into four channels ending in 1.1 mm diameter islet chambers, each of which was capable of holding five to eight islets, increasing biological throughput of the device compared with previous designs (19,20). The chambers were maintained at 37 ± 0.5°C using a thermofoil heater, thermocouple, and control system (17). The glucose concentration delivered to the chambers was calibrated by addition of fluorescein to the high-glucose buffer and varying the reservoir heights as described previously (22). In brief, the normalized concentration of fluorescein was plotted against reservoir height and a linear calibration curve was fit, allowing the heights of the reservoirs to be calculated to achieve a desired glucose concentration at the islet chambers.

To measure $[Ca^{2+}]_i$, 1 μL of 5 mM Fura 2 acetoxymethyl ester in DMSO and 1 μL of Pluronic F-127 in DMSO were added to 1.998 mL of RPMI 1640 medium. Islets were incubated in this solution for 40 min at 37°C and 5% CO_2. After incubation, islets were rinsed in prewarmed 10 mM BSS and loaded into the microfluidic device by hand.

The epifluorescent $[Ca^{2+}]_i$ imaging system is the same as described previously (20,22) with the addition of a motorized *xy* stage to move between islet chambers. Imaging and stage movement was controlled by a custom LabVIEW program. The glucose feedback system is as described previously (19,20). In brief, two images were taken using excitation wavelengths of 340 ± 5 and 380 ± 5 nm for 150 ms each. The ratio of the fluorescent intensities at 520 ± 20 nm from each islet were calculated for the two wavelengths to obtain the 340/380 ratio. $[Ca^{2+}]_i$ of islets was calculated from the 340/380 ratio using calibration values determined by previously reported methods (24). Once the first chamber was imaged, the motorized stage moved the microfluidic device to image the second chamber, taking ∼2 s to image and move for each chamber. This process was repeated for all four chambers, taking ∼8 s. The next round of imaging began ∼13 s later, meaning $[Ca^{2+}]_i$ was measured for all islets every 20 s. For each round of imaging, Ca_{avg} was used to calculate the glucose concentration to be delivered via a sigmoidal calibration curve. The parameters defining the

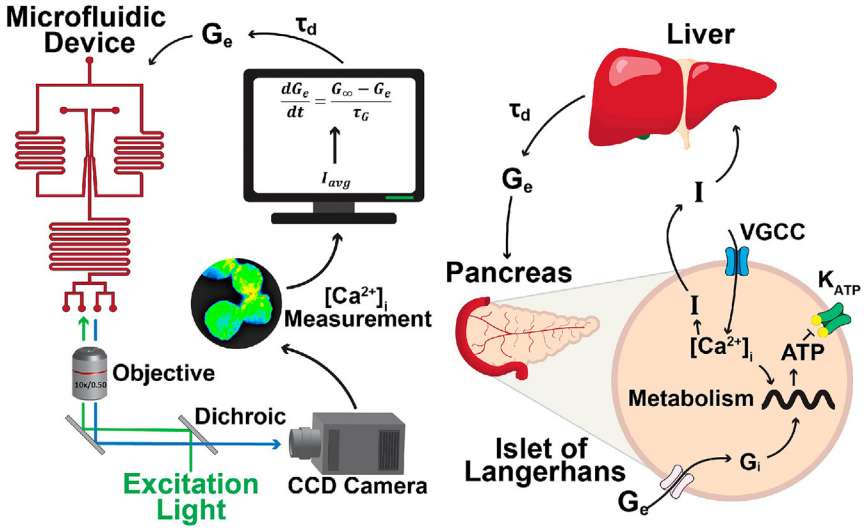

FIGURE 1 Illustration of the closed-loop feedback system employed with murine islets studied in a microfluidic system (*left*), and its relationship to physiological interactions (*right*). Starting from the left, variable glucose is delivered to groups of islets via a microfluidic device. The $[Ca^{2+}]_i$ of each islet is measured from which an average insulin (I_{avg}) is calculated and used to update the glucose feedback delivered to the islets. The right side depicts closed-loop negative glucose feedback with the integrated oscillator model.

glucose feedback were estimated at the time of each experiment and were dependent on each islet population. The glucose concentration delivered varied between a minimum and maximum value which was defined before initiating glucose feedback.

Mathematical model

The mathematical model used, shown in Fig. 1 and previously introduced in (19), combines a model for β cell bursting activity (25) with a model of glucose negative feedback, producing a closed-loop system for insulin secretion and its effect on glucose (18). The bursting model, known as the integrated oscillator model (25,26), consists of 8 differential equations for membrane potential, the activation of a delayed rectifying K^+ current, concentrations of free Ca^{2+} in the cytoplasm (the variable Ca used below and throughout the paper), in the endoplasmic reticulum, and in the mitochondria, and concentrations of adenosine diphosphate, fructose 6-phosphate, and fructose 1,6-biphosphate. It bidirectionally couples a metabolic oscillator and an electrical oscillator. Metabolism of glucose produces ATP that inhibits K(ATP) channels, depolarizing the plasma membrane and thus influencing the electrical oscillator. The resulting excess Ca in the cytoplasm promotes PDH activity, increasing flux through glycolysis and thus influencing the metabolic oscillator. We assume that a single islet is representative of all β cells within the islet due to intraislet synchronization mediated by gap junctions.

The rate of insulin secretion for each islet changes over time according to:

$$\frac{dI}{dt} = \frac{I_\infty - I}{\tau_I} \tag{1}$$

where τ_I is a time constant and I_∞ is the equilibrium secretion rate, given by an increasing function of Ca past a threshold Ca_{thr}:

$$I_\infty = \begin{cases} I_{\text{slope}}(Ca - Ca_{\text{thr}}) & Ca \geq Ca_{\text{thr}} \\ 0 & Ca < Ca_{\text{thr}} \end{cases}. \tag{2}$$

In the negative feedback loop, the extracellular glucose concentration is modulated by the average insulin secretion from the population of N islets, $I_{\text{avg}} = \frac{1}{N}\sum_{j=1}^{N} I_j$, where I_j is the insulin secretion rate from islet j. After a time delay to account for glucose circulation in the blood, the islet population then senses the new extracellular glucose concentration which coordinates their activity. The extracellular glucose concentration changes in time according to:

$$\frac{dG_e}{dt} = \frac{G_\infty - G_e}{\tau_G} \tag{3}$$

where τ_G is a time constant and G_∞ is the asymptotic extracellular glucose response function. This is a decreasing sigmoidal function of I_{avg} with time delay τ_d:

$$G_\infty = G_{\min} + \frac{G_{\max} - G_{\min}}{1 + \exp\left(\frac{I_{avg}(t - \tau_d) - \hat{I}}{S_G}\right)}. \tag{4}$$

The maximum extracellular glucose concentration is $G_{\max}$ and the minimum is $G_{\min}$. The value of the function is half way between these two extremes when $I_{\text{avg}} = \hat{I}$. Parameter S_G determines the steepness of the response function. Eqs. 3 and 4 are the same for the experiment and model as described previously in (19). The parameters $G_{\max}$, $G_{\min}$, and $\hat{I}$ are defined by each experiment individually while they are fixed between simulations in the model.

The values of parameters in Eqs. 1, 2, 3, and 4 and those that differ from values used in (19,25) are given in Table 1. The parameters for the maximum K(ATP) channel conductance ($g_{K(ATP)}$) and glucose sensitivity (V_{gk}) were varied to create a heterogeneous islet population with slow and compound bursting modes and periods ranging from 3 to 8 min.

Mean-field model

To understand the dynamics of the closed-loop feedback system, a two-variable model was constructed with two differential equations for G_e and average Ca (which reflects the average insulin concentration). The time dynamics of the average Ca (Ca_{avg}) are described by:

$$\frac{dCa_{\text{avg}}}{dt} = \frac{C_\infty - Ca_{\text{avg}}}{\tau_C} \tag{5}$$

TABLE 1 Fixed parameter values for the full model

$\tau_I = 10,000$ ms	$I_{\text{slope}} = 1000\ \mu\text{M}^{-1}$	$Ca_{\text{thr}} = 0.1\ \mu$M	$\tau_G = 50,000$ ms
$G_{\min} = 7$ mM	$G_{\max} = 13$ mM	$\hat{I} = 30$	$S_G = 1$

where τ_C is a time constant and C_∞ is an increasing sigmoid function of glucose, reflecting the fact that Ca in islet β cells is larger in higher glucose concentrations:

$$C_\infty = v_C \frac{G_e^{n_C}}{k_C^{n_C} + G_e^{n_C}} + C_{\min} . \quad (6)$$

Extracellular glucose concentration behaves inversely to Ca_{avg}. When Ca_{avg} is low there is less insulin secretion, so the glucose concentration increases. When Ca_{avg} is high there is more insulin secretion, causing the glucose concentration to decline due to actions of the liver. Thus, the equation for extracellular glucose concentration in the mean-field model is adapted from the full model and given by:

$$\frac{dG_e}{dt} = \frac{G_\infty - G_e}{\tau_G} \quad (7)$$

where τ_G is a time constant and G_∞ is a decreasing sigmoid function of Ca_{avg} with a time delay τ_d:

$$G_\infty = -v_G \frac{Ca_{\text{avg}}^{n_G}(t - \tau_d)}{k_G^{n_G} + Ca_{\text{avg}}^{n_G}(t - \tau_d)} + G_{\max} \quad (8)$$

The parameters of the sigmoid functions were determined based on time courses of variables from the full model. To set parameter values of the C_∞ function, the model was used to simulate 50 islets at 7, 8, 9, 10, 11, 12, and 13 mM constant glucose concentrations each for 30 min, as shown in Fig. 2 *A*. The extracellular glucose concentration is shown in red, and Ca_{avg} for the 50 islets is shown in black. The average of Ca_{avg} was calculated for each glucose concentration and is shown as black circles in Fig. 2 *B*. The C_∞ function (*blue curve* in Fig. 2 *B*) was then fit to these data using the method of least squares. The resulting parameter values are given in Table 2.

In the full model, the glucose response function is based on the average insulin secretion, while in the reduced model, G_∞ is a function of Ca_{avg}. To convert average insulin secretion in the full model to Ca_{avg}, we use the following linear transformation:

$$Ca_{\text{avg}} = p_c I_{\text{avg}} + C_{\text{base}} . \quad (9)$$

The G_∞ function in the mean-field model was then fit to the transformed glucose response curve using the method of least squares.

To introduce noise in the mean-field model, the deterministic system was converted to a stochastic system. Noise is added to the Ca_{avg} equation to replicate the effects observed in the full model from a small number of heterogeneous islets on Ca_{avg}. The equation for Ca_{avg} becomes:

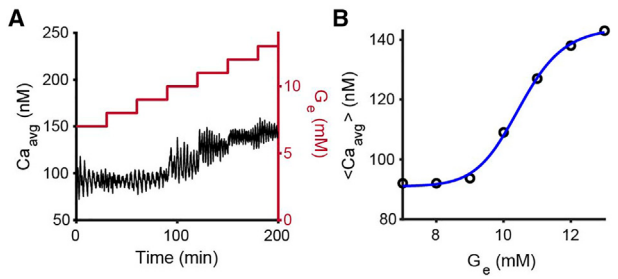

FIGURE 2 Parameter fitting for the C_∞ function. (*A*) In a full model simulation of 50 islets, G_e (*red*) was increased from 7 to 13 mM and held constant at each value for 30 min. In response to increasing G_e, Ca_{avg} (*black*) increases. (*B*) For each value of G_e, the average Ca_{avg} value was calculated and plotted as black circles. The C_∞ function was fit to the points using the method of least squares (*blue curve*).

TABLE 2 Parameter values for the mean-field model

$\tau_C = 100,000$ ms	$v_C = 53.13$ nM	$n_C = 15.92$	$k_c = 10.48$ mM
$C_{\min} = 91$ nM	$\tau_G = 50,000$ ms	$v_G = 6.01$ mM	$n_G = 67.20$
$\sigma = 8$	$k_G = 107.99$ nM	$G_{\max} = 13$ mM	$p_c = 1.6$ mM
$C_{\text{base}} = 30$ nM			

$$\frac{dCa_{\text{avg}}}{dt} = \frac{C_\infty - Ca_{\text{avg}}}{\tau_C} + \sigma W(t) \quad (10)$$

where $W(t)$ is white Gaussian noise with mean 0 and variance 1. The parameter σ scales the variance of $W(t)$ and is set to a value that ensures Ca_{avg} is nonnegative and within range of what is seen for small islet populations in the full model. All parameter values for the mean-field model are shown in Table 2.

Data analysis

Spectral analysis was used to calculate the oscillation period of the coordinated system after feedback was turned on. Specifically, a fast Fourier transform was taken of the Ca_{avg} signal once G_e was allowed to vary according to the feedback model. The period corresponding to the primary peak was taken to be the closed-loop oscillation period. If the closed-loop period was ∼5 min, we considered this a fast closed-loop oscillation that reflects synchronization of the islet oscillators. If the closed-loop period was $\sim 2\tau_d$ min or longer, we considered the system to be exhibiting slow coordinated oscillations. There was no ambiguity between the two oscillation periods since we used only time delays that resulted in slow oscillation periods much greater than the fast synchronized oscillation period.

RESULTS

We previously showed that negative feedback can synchronize small populations of three to six islets, both with and without a time delay in the negative feedback, resulting in closed-loop oscillations in the islet population with period of ∼5 min (19,20). With a time delay of several (up to 6) minutes in the negative feedback, an additional form of coordination can occur in which islet oscillations are grouped together into slow episodes. The period of the slow oscillations increases linearly with the time delay, while the period of the fast oscillations remains independent of the time delay (19). Do slow closed-loop oscillations still exist even with considerably larger time delays? How does the size of the islet population involved in the negative feedback impact the likelihood of fast versus slow closed-loop oscillations? To address these questions, we begin with computer simulations of islet populations of various sizes subject to negative feedback with a longer 10 min time delay.

Fast and slow closed-loop oscillations exist for long time delays

We first describe computer simulations with a small population of five islets with a range of native oscillation periods, similar to simulations performed in a previous study (19). In the simulations, the external glucose concentration (G_e) was

initially held constant at 10 mM and the islets oscillated out of phase. After 20 min, the feedback was turned on with a time delay of $\tau_d = 10$ min and G_e varied according to Eq. 3. The Ca^{2+} concentration averaged over the islet population (Ca_{avg}) was tracked as a proxy for insulin secretion. The oscillations in Ca_{avg} for the first 20 min were small and irregular, indicating little coherence in the oscillations of the five model islets. Once the feedback was turned on at $t =$ 20 min, however, the model islets produced fast closed-loop oscillations reflecting islet synchronization. As a result, there are oscillations in G_e and the oscillations in Ca_{avg} are larger and more regular than when G_e was fixed, with period of $\sim$ 4 min (Fig. 3 *A*). In Fig. 3 *B*, the same population of five model islets produced slow oscillations with a $\sim$ 25 min period once the feedback was turned on. This slow rhythm is evident in both the external glucose and Ca_{avg}, particularly when a moving average of Ca_{avg} with window size of 3 min is calculated and superimposed. Because these simulations differed only in their initial conditions, and not parameter values, this indicates that the system with the long time delay $\tau_d = 10$ min is bistable.

Slow oscillations become better defined and more prevalent when the islet number is increased

We next examined how the size of the islet population affects the rhythm generated by the closed-loop system. Groups of murine islets were isolated and loaded into the microfluidic device outlined in (Fig. 1). In these experiments, glucose was initially held constant at 10 mM for a period of ~20 min to confirm that islets were oscillating. During this time interval Ca_{avg} had small, irregular oscillations indicating a lack of synchronization (Fig. 4), like those seen in model simulations (Fig. 3). The feedback was then turned on with a delay of $\tau_d = 10$ min and variable G_e delivered as described in the materials and methods and (19). *Ca* was measured for each islet and Ca_{avg} calculated and used in the glucose delay differential equation (Eq. 7). In this closed-loop configuration, the Ca_{avg} time course became more regular and the oscillations had larger amplitude, indicating synchronization. In addition, there were accompanying glucose oscillations induced by the oscillations in Ca_{avg} through the feedback mechanism. As with the model simulations, the number of islets used to calculate Ca_{avg} in the experiments affected the synchronized period, with a group of 5 islets producing an oscillation period of $\sim$ 5 min (Fig. 4 *A*), and a group of 20 islets producing a period of $\sim$ 27 min (Fig. 4 *B*). This behavior reflects that predicted by model simulations whereby larger groups of islets produce better defined oscillations in G_e and Ca_{avg} (Fig. 3 *C*).

An additional effect of increasing the number of islets in the population is that the prevalence of slow closed-loop oscillations increased. This was true in both the model simulations and in experiments. In the model, 50 simulations for islet populations of 5, 10, 15, or 20, and a time delay of 10 min were performed. The percentage of simulations resulting in slow closed-loop oscillations increased linearly from 8 to 74% (slope $m = 4.36$ and $R^2 = 0.97$) as the size of the population increased from 5 to 20 islets. Thus, the system appears to be bistable for all population sizes and time delays tested with the model, and slow oscillations are most likely when the population size is large. These

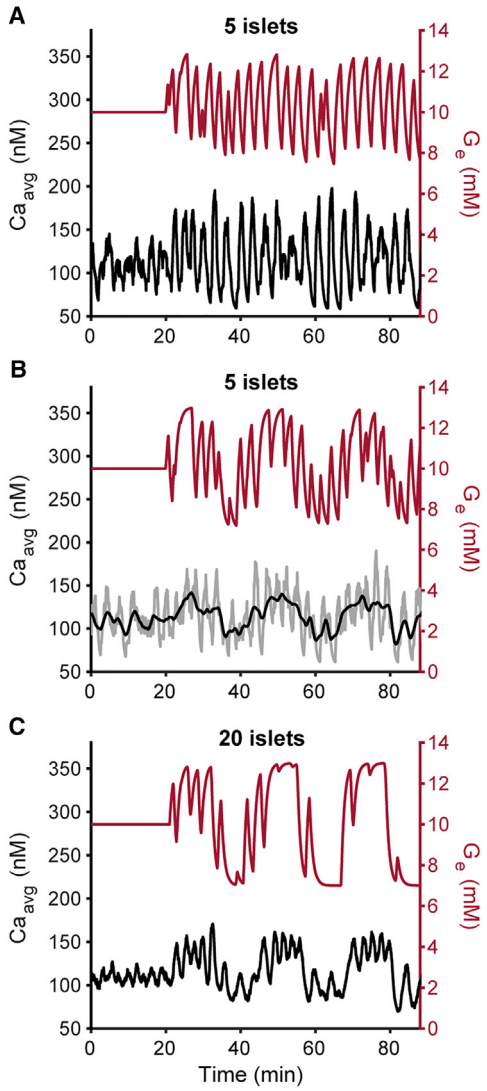

FIGURE 3 Model simulations with a time delay of $\tau_d = 10$ min in the glucose feedback. Red curves show G_e and black show Ca_{avg}. (*A*) G_e was initially held constant at 10 mM and the five model islets oscillated out of phase due to heterogeneity in their natural periods. After 20 min, G_e was allowed to vary according to the feedback model. The islets synchronized to a fast $\sim$ 4 min period. (*B*) The same five islets but with different initial conditions synchronized to a slow $\sim$ 25 min period once feedback was turned on, indicating the system is bistable. Here, the gray line represents Ca_{avg} and the black line represents the moving average of Ca_{avg} with a 3 min window to make the slow oscillation more apparent. (*C*) A population of 20 model islets synchronized to a slow oscillation period of $\sim$ 24 min once feedback was turned on.

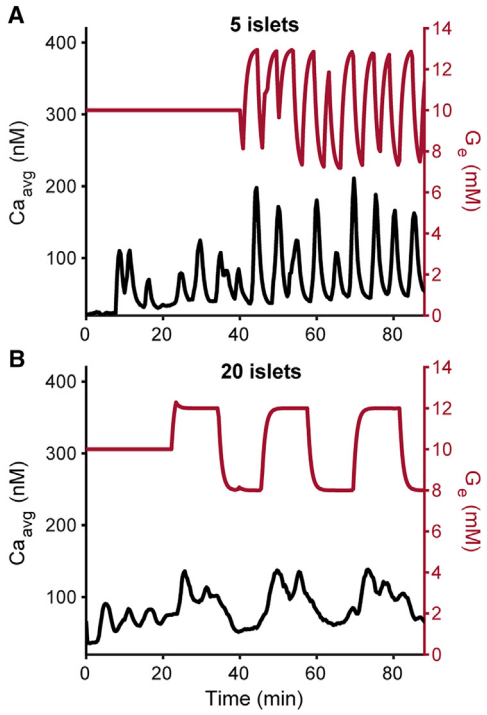

FIGURE 4 Oscillations in populations of murine islets with a time delay of $\tau_d = 10$ min in the glucose feedback. Red curves are the glucose concentration delivered to the islets, G_e. Black curves are Ca_{avg} for the islet population. (*A*) G_e was initially held constant at 10 mM and the five islets oscillated out of phase due to heterogeneity in their natural periods, resulting in small and irregular fluctuations in Ca_{avg}. After 40 min, glucose feedback was started, yielding larger oscillations in Ca_{avg} at a period of ~ 5 min. (*B*) A population of 20 islets yielded a slow closed-loop oscillation with period of ~ 27 min once glucose feedback was started.

predictions are mirrored in populations of murine islets. Experiments with 20 or more islets and a time delay of 10 min showed a slow closed-loop oscillation in all cases examined ($n = 4$), while 5–6 islets and a 10 min time delay always showed synchronization to a fast period ($n = 5$). These experimental results for large populations of islets are shown in the supporting material (Figs. S1–S4) and for small populations of islets (Figs. S5–S9). This result confirms that, for large islet populations, we expect to see slow closed-loop oscillations a majority of the time.

A mean-field model can explain the slow closed-loop oscillations

The square-wave appearance of G_e and Ca_{avg} during the slow closed-loop oscillations shown in Fig. 3 *C* motivates a way to reduce the complexity of the system to facilitate understanding of the genesis of the slow oscillations. This mean-field model, described in materials and methods, is based on the fact that Ca_{avg} will be high when the glucose level is high (due to the stimulatory action of glucose on islet β cells), and that the glucose level should drop to a low value when Ca_{avg} is high (due to the positive effect of insulin on glucose uptake by the liver). This information is built into the equilibrium functions for both variables, as described in materials and methods. Thus, the mean-field model consists of only two variables, Ca_{avg} and G_e, with a time delay in the G_e equation, and is meant to approximate results from simulations of the full model with the larger islet populations shown in Fig. 3 *C*.

With the time delay set to 0, the mean-field model settles to a stable equilibrium. This reflects the case of no slow oscillations in the full model, which indeed only exhibits slow closed-loop oscillations when there is a time delay. Oscillations begin in the mean-field model with a time delay of approximately $\tau_d = 0.073$ min ($\sim$4 s). With this value of the delay there is a supercritical Hopf bifurcation, and for larger values the model produces a stable limit cycle oscillation. Fig. 5 *A* shows oscillations produced by the mean-field model with a time delay of 10 min. The oscillation period, ~ 24 min, is considerably longer than the time delay. We compare these oscillations to slow closed-loop oscillations in the full model with the same time delay and with a large population of 50 islets in Fig. 5 *B*. The mean-field and full model oscillations are quite similar, and in particular have similar periods of $\sim$24 min. The trajectories are also compared in the phase plane of Ca_{avg} and G_e (Fig. 5 *C*). The nullclines for Ca_{avg} and G_e in the mean-field model are shown in orange and blue, respectively, and the single equilibrium formed at their intersection is unstable. The mean-field trajectory corresponding to Fig. 5 *A* is shown in black in the phase plane, and that for the full model corresponding to Fig. 5 *B* is shown in gray. The full model trajectory appears much noisier, since Ca_{avg} is the average of the Ca^{2+} concentrations of 50 model islets, which are only partially synchronized into slow episodes. Still, despite that, the full model trajectory has the basic shape of the mean-field limit cycle.

The similarity between slow oscillations in the full model and those in the mean-field model persists for other delay times, as can be seen by comparing oscillation periods of the mean-field model (*blue curve*) with those of the full model (*orange curve*) in Fig. 5 *D*. The oscillation period increases with the time delay in an almost linear fashion and at a similar rate in both models, with a slope of ≈ 2. The reason for this slope in the mean-field model is that it takes τ_d min for one variable to sense and respond to a change in the other, and a change occurs twice during each oscillation (for example, when the average glucose variable goes from low to high, and then later from high back to low). Thus, the oscillation period is approximately $2\tau_d$. The similarities in phase plane trajectories and the change in oscillation period with the time delay strongly suggests that the mechanism of slow closed-loop oscillations in the full model is the same as that of oscillations in the mean-field model. That is, it is a limit cycle oscillation induced by the delay in negative feedback, as seen in delay differential equation models for other biological systems, including circadian rhythms (27,28) and ultradian rhythms in hormone secretion (29).

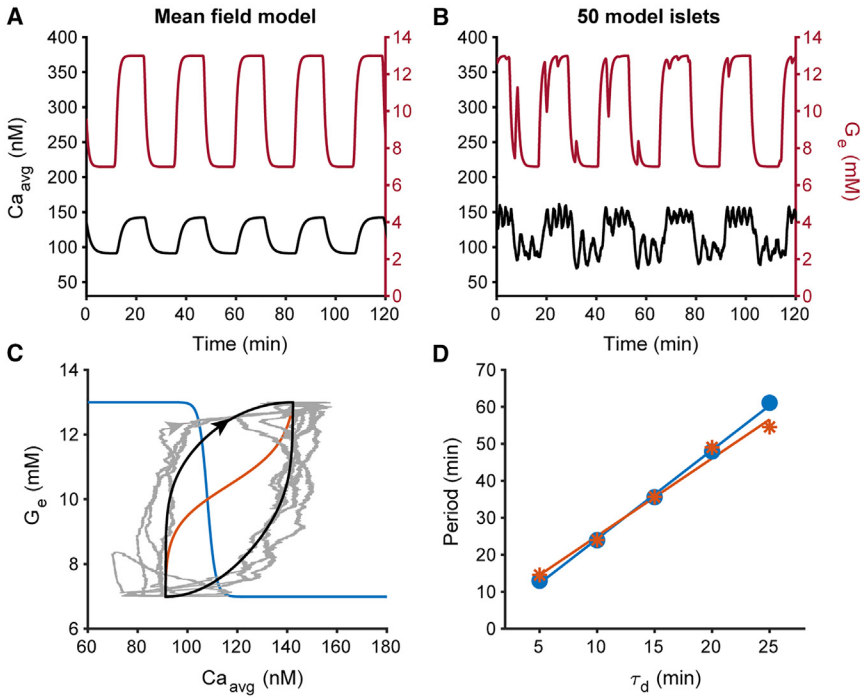

FIGURE 5 The mean-field model captures the dynamics of slow closed-loop oscillations for large islet population in the full system. (*A*) The mean-field model with a 10 min time delay produces oscillations with an $\sim$ 24 min period. (*B*) A population of 50 model islets with a 10 min time delay in the full system produce slow oscillations that are qualitatively similar to those seen in the mean-field model. (*C*) In phase space, the trajectories of the mean-field model (*black curve*) and the full model (*gray curve*) show considerable agreement. The Ca_{avg} and G_∞ nullclines for the mean-field model are shown in orange and blue, respectively, and the arrows indicate the direction of the trajectories. (*D*) The period of the oscillations in the mean-field model increases with the time delay (*blue curve*, slope $m = 2.41$ and $R^2 = 0.99$). The trend is nearly identical to what is seen when increasing the time delay in the full model with 50 islets (*orange curve*, slope $m = 2.10$ and $R^2 = 0.99$).

The mean-field model gives insights into the mechanism of bistability

Oscillations in the mean-field model correspond to slow closed-loop oscillations in the full system, while a stable equilibrium state corresponds to fast closed-loop oscillations. How can the mean-field model account for bistability between the two? We believe that this can be attributed to the effects of noise. In the full model there is no stochastic element, but there is heterogeneity among the islet oscillators, which impacts the establishment of oscillator coherence, and which is a particularly strong influence when the sample size is small (e.g., five islets as in Fig. 3). To replicate this influence in the mean-field model, we introduced stochastic additive white Gaussian noise to the Ca_{avg} equation in the mean-field model. The variance of the noise is chosen to give a similar scale to Ca_{avg} in the full model under constant glucose and to ensure the function value is never negative. When white noise is added to Ca_{avg} in the mean-field model with a 3 min time delay (see materials and methods), the result is random jitter interspersed with slow oscillations (Fig. 6 *A*). This intermittency reflects perturbations away from periodic limit cycle motion, so after one or two cycles around the limit cycle, the trajectory is pushed off for some time before ultimately returning to produce one or more slow oscillations. Thus, although the deterministic mean-field model is not bistable, the noise introduces a nonoscillatory state that gives the appearance of bistability in the noisy mean-field model. This competition between slow oscillations and jitter is also seen with a small number of islet oscillators in the full model and in the experimental system as in Fig. 6, *B* and *C*, respectively. Here, we see five islets with a 3 min time delay jump between producing fast and slow oscillations in both systems. The fast oscillations in the full and experimental systems are due to intrinsic oscillations in the islets, thus they have more organization than the jitter in the noisy mean-field model, but the combination of slow oscillations with intervening fast events is similar. This behavior occurs less frequently as islet number increases, supporting the idea that it is a ramification of small sample size. Thus, we propose that the bistability observed in the full model simulations and in vitro experiments is due to the heterogeneity in islet oscillation periods interfering with the slow rhythm that results from the delayed negative feedback, allowing the islet oscillations to synchronize to yield fast closed-loop oscillations. This proposal for the mechanism for bistability would account for the increase in the rate of occurrence of slow closed-loop oscillations with an increase in the number of islets; the effects of heterogeneity diminish when more islets participate in the feedback.

DISCUSSION

Individual islets provide their own rhythm of activity that we refer to as fast oscillations. Our previous work established that fast islet oscillations can be synchronized through feedback from the liver and/or other target tissue that participate in glucose homeostasis, providing a unified fast rhythm in the population (20). Such rhythms have been observed numerous times in plasma insulin measurements from mice (8,13), rats (9), dogs (9), monkeys (10), and humans (7,11,30,31), and

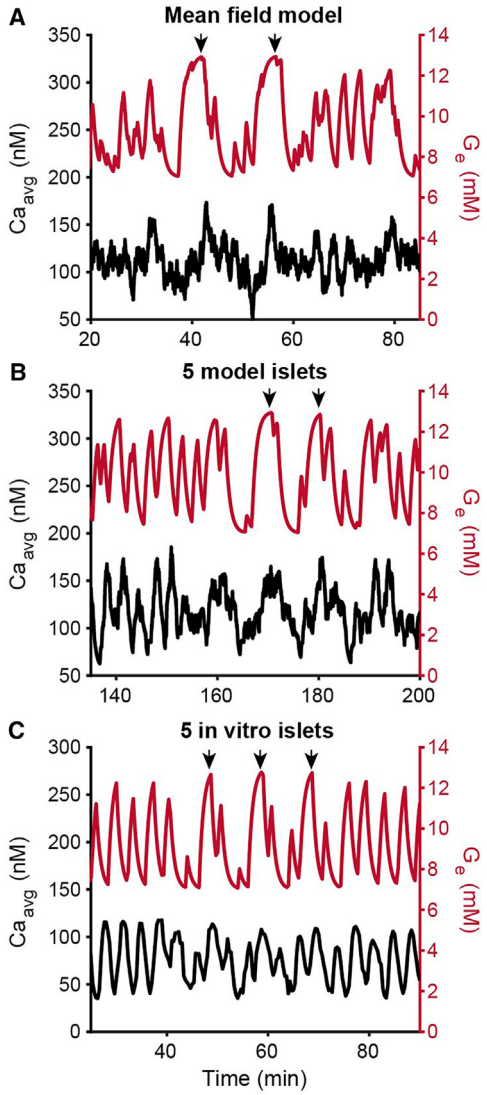

FIGURE 6 Adding noise in the mean-field model resembles behavior seen in small populations of model and murine islets. (*A*) When stochastic white Gaussian noise is added to the Ca_{avg} equation in the mean-field model to reflect a small islet population, the trajectory is pushed away from the limit cycle. Black arrows indicate where the slow oscillation solution is evident. Small islet populations of five model islets (*B*) and five murine islets (*C*) with a 3 min time delay produce similar behavior, with slow oscillations interspersed within fast oscillations.

some studies in which glucose was sampled also found fast glucose oscillations (30,31). We also showed previously that synchronization through closed-loop feedback is robust to time delays, and that these delays can induce a slower rhythm that is bistable with the fast rhythm (19). Time delays would be expected due to the time required for changes in the local glucose concentration due to the action of the liver to diffuse through the circulation and reach individual islets, and are often employed in models of ultradian rhythms in blood insulin levels (32–34).

In this study, we determined the mechanism for the slow rhythm, as well as an explanation for the bistability between the fast and slow rhythms. Using a reduced model, we showed that the slow rhythm is of the same nature as other delayed negative feedback systems in which oscillations are expected to occur only when the delay is sufficiently large (29,35). This agrees with our previous findings in a small (∼5 islets) population that a slow rhythm was observed with a delay as small as 1 min, but was never observed when there was no time delay in the feedback (19). We also showed that the fast rhythm often seen in the islet population, even with a substantial time delay, could be explained by the use of small islet populations in the closed-loop system. When larger islet populations (∼20 islets) were studied, the slower rhythm was preferentially observed. With a 5-islet population the heterogeneity in intrinsic islet oscillation periods can very easily disrupt the slow rhythm provided by the delayed negative feedback, much like adding noise in the model of the reduced system (Fig. 6). The coefficient of variation in the intrinsic islet periods declines with the number of islets in the population, so is less likely to disturb the slow rhythm induced by the delayed feedback. For this reason, it is more likely to observe a slow rhythm in a 20-islet population than in a 5-islet population, as we found both in model simulations and in vitro experiments.

The bistability that we demonstrated previously with populations of 5–6 islets can therefore be thought of as a tug-of-war between the effects of the delay in the negative feedback, which would induce a slow rhythm with period approximately twice that of the delay, and the effects of synchronization of the intrinsic oscillators, which would have a period near the mean of the intrinsic islet periods. The winner of the tug-of-war depends on the state of the islet variables (e.g., voltage, Ca^{2+} concentration, ATP levels) when the feedback is established. In fact, we observed cases where the islet population moved back and forth between fast and slow rhythms (Fig. 6). With larger islet populations it becomes more likely that the slow rhythm is expressed, so the bistability becomes less evident. Indeed, in our experiments we found no cases of pure fast oscillations with populations of 20 islets. In the large populations of islets present in vivo, the model suggests that slow oscillations would typically be present, and indeed several in vivo plasma insulin measurements show insulin oscillations with periods of 10 min or greater, often mixed in with faster insulin oscillations (10,11,31).

The presence of slow oscillations does not discount the ∼5 min rhythmicity of the individual islets. Indeed, the slow rhythm that we observed in our simulations and experiments is typically composed of episodes of faster oscillations. The primary effect of the feedback is then to change the timing of the individual islet oscillations, rather than to change their oscillation period. In the Fourier power spectrum of Ca_{avg} for both model and murine islets, there was typically a peak near 5 min and another at $2\tau_d$ or greater. (This is evident in the experimental figures shown in the text and in the supporting figures as fast oscillations riding on slower oscillations.) Which one dominates determined

whether we categorized the rhythm as fast or slow, and often the two peaks were similar in magnitude. The episodes of fast oscillations grouped into slower episodes are reminiscent of "compound bursting" that is often observed in the electrical activity of individual islets, although in that case the fast component typically has a period of less than 30 s while the period of the slow component is ∼5 min (36). In both cases, the rhythm is due to a combination of a mechanism for fast oscillations interacting with a mechanism for slower oscillations.

An important class of slow oscillations in the plasma insulin and glucose concentration is the ultradian oscillations. These have been characterized in humans under a variety of conditions (37–42). The oscillations have periods ranging from 50 min to 2 h, and tend to be smaller in amplitude in older individuals (43) and in individuals who have impaired glucose tolerance or have noninsulin-dependent diabetes mellitus (44). Could the mechanism for the ultradian rhythms be similar to that of the slow rhythms that we have characterized? Mathematical modeling has suggested that the mechanism is similar, using closed-loop feedback between insulin-secreting islets and glucose-regulating target tissue (32–34,45). However, the time delay needed for ultradian rhythms (∼ 30 min) is substantially larger than the delays that we considered here. We speculate that, with a 30 min time delay, we would see slow oscillations with period of approximately 1 h, i.e., ultradian rhythms, but there are technical challenges to the in vitro experiments that must be overcome to test this hypothesis.

There are several lines of evidence for the importance of insulin rhythmicity. In humans, most of the insulin that is secreted by islets (between 70 and 80%) is secreted in pulses (46,47), and it has been demonstrated that hepatic insulin action is enhanced when the insulin signal is pulsatile rather than constant (2,48). In individuals with type II diabetes and their near relatives, the fast (3), as well as ultradian (49), insulin rhythms are disrupted. The pulsatility of individual islets is a key element ensuring insulin pulsatility, but since islets are not directly connected another element that is required is a synchronization mechanism. The current study, along with previous ones (18–20), provides a characterization of one of two likely mechanisms. It is likely that both mechanisms, closed-loop feedback with the liver and neural input from pancreatic ganglia, contribute to islet synchronization in the intact animal.

SUPPORTING MATERIAL

Supporting material can be found online at https://doi.org/10.1016/j.bpj.2024.07.028.

AUTHOR CONTRIBUTIONS

Research design, N.B., J.T., M.G.R., and R.B.; performance of research, N.B., J.T., and I.-A.W.; data analysis, N.B., J.T., M.G.R., and R.B.; manuscript writing, N.B., J.T., M.G.R., and R.B.

ACKNOWLEDGMENTS

This work was supported by a grant from the National Institutes of Health (R01 DK080714).

DECLARATION OF INTERESTS

The authors declare no competing interests.

REFERENCES

1. Komjati, M., P. Bratuschmarrain, and W. Waldhäusl. 1986. Superior efficacy of pulsatile versus continuous hormone exposure on hepatic glucose production in vitro. *Endocrinology.* 118:312–319.
2. Matveyenko, A. V., D. Liuwantara, …, P. C. Butler. 2012. Pulsatile portal vein insulin delivery enhances hepatic insulin action and signaling. *Diabetes.* 61:2269–2279.
3. O'Rahilly, S., R. C. Turner, and D. R. Matthews. 1988. Impaired pulsatile secretion of insulin in relatives of patients with non-insulin-dependent diabetes. *N. Engl. J. Med.* 318:1225–1230.
4. Satin, L. S., P. C. Butler, …, A. S. Sherman. 2015. Pulsatile insulin secretion, impaired glucose tolerance and type 2 diabetes. *Mol. Aspect. Med.* 42:61–77.
5. Rorsman, P., and F. M. Ashcroft. 2018. Pancreatic β-cell electrical activity and insulin secretion: Of mice and men. *Physiol. Rev.* 98:117–214.
6. Cook, D. L. 1983. Isolated islets of Langerhans have slow oscillations of electrical activity. *Metabolism.* 32:681–685.
7. Song, S. H., S. S. McIntyre, …, P. C. Butler. 2000. Direct measurement of pulsatile insulin secretion from the portal vein in human subjects. *J. Clin. Endocrinol. Metab.* 85:4491–4499.
8. Nunemaker, C. S., D. H. Wasserman, …, L. S. Satin. 2006. Insulin secretion in the conscious mouse is biphasic and pulsatile. *Am. J. Physiol.* 290:E523–E529.
9. Matveyenko, A. V., J. D. Veldhuis, and P. C. Butler. 2008. Measurement of pulsatile insulin secretion in the rat: direct sampling from the hepatic portal vein. *Am. J. Physiol.* 295:E569–E574.
10. Goodner, C. J., F. G. Hom, and D. J. Koerker. 1982. Hepatic glucose production oscillates in synchrony with the islet secretory cycle in fasting rhesus monkeys. *Science.* 215:1257–1260.
11. Lang, D. A., D. R. Matthews, …, R. C. Turner. 1981. Brief, irregular oscillations of basal plasma insulin and glucose concentrations in diabetic man. *Diabetes.* 30:435–439.
12. King, B. F., J. A. Love, and J. H. Szurszewski. 1989. Intracellular recordings from pancreatic ganglia of the cat. *J. Physiol.* 419:379–403.
13. Nunemaker, C. S., M. Zhang, …, L. S. Satin. 2005. Individual mice can be distinguished by the period of their islet calcium oscillations: is there an intrinsic islet period that is imprinted in vivo? *Diabetes.* 54:3517–3522.
14. Tang, S. C., L. Baeyens, …, M. S. German. 2018. Human pancreatic neuro-insular network in health and fatty infiltration. *Diabetologia.* 61:168–181.
15. Kirchgessner, A. L., and J. E. Pintar. 1991. Guinea pig pancreatic ganglia: Projections, transmitter content, and the type-specific localization of monoamine oxidase. *J. Comp. Neurol.* 305:613–631.
16. Ushiki, T., and S. Watanabe. 1997. Distribution and ultrastructure of the autonomic nerves in the mouse pancreas. *Microsc. Res. Tech.* 37:399–406.
17. Adablah, J. E., R. Vinson, …, R. Bertram. 2019. Synchronization of pancreatic islets by periodic or non-periodic muscarinic agonist pulse trains. *PLoS One.* 14:e0211832.

18. Pedersen, M. G., R. Bertram, and A. Sherman. 2005. Intra- and inter-islet synchronization of metabolically driven insulin secretion. *Biophys. J.* 89:107–119.
19. Bruce, N., I. A. Wei, …, R. Bertram. 2022. Coordination of pancreatic islet rhythmic activity by delayed negative feedback. *Am. J. Physiol.* 323:E492–E502.
20. Dhumpa, R., T. M. Truong, …, M. G. Roper. 2014. Negative feedback synchronizes islets of Langerhans. *Biophys. J.* 106:2275–2282.
21. Roper, M. G., J. G. Shackman, …, R. T. Kennedy. 2003. Microfluidic chip for continuous monitoring of hormone secretion from live cells using an electrophoresis-based immunoassay. *Anal. Chem.* 75:4711–4717.
22. Yi, L., X. Wang, …, M. G. Roper. 2015. Integrated perfusion and separation systems for entrainment of insulin secretion from islets of Langerhans. *Lab Chip.* 15:823–832.
23. Ferry, M. S., I. A. Razinkov, and J. Hasty. 2011. Methods in Enzymology. *In* chapter fourteen - Microfluidics for Synthetic Biology: From Design to Execution Elsevier, pp. 295–372.
24. Grynkiewicz, G., M. Poenie, and R. Y. Tsien. 1985. A new generation of Ca2+ indicators with greatly improved fluorescence properties. *J. Biol. Chem.* 260:3440–3450.
25. Marinelli, I., T. Vo, …, R. Bertram. 2018. Transitions between bursting modes in the integrated oscillator model for pancreatic β-cells. *J. Theor. Biol.* 454:310–319.
26. Bertram, R., I. Marinelli, …, A. S. Sherman. 2023. Deconstructing the integrated oscillator model for pancreatic β-cells. *Math. Biosci.* 365:109085.
27. Scheper, T., D. Klinkenberg, …, J. van Pelt. 1999. A mathematical model for the intracellular circadian rhythm generator. *J. Neurosci.* 19:40–47.
28. Bertram, R., M. Egli, …, M. E. Freeman. 2006. A mathematical model for the mating-induced prolactin rhythm of female rats. *Am. J. Physiol.* 290:E573–E582.
29. Walker, J. J., J. R. Terry, and S. L. Lightman. 2010. Origin of ultradian pulsatility in the hypothalamic-pituitary-adrenal axis. *Proc. Biol. Sci.* 277:1627–1633.
30. Mao, C. S., N. Berman, …, E. Ipp. 1999. Glucose entrainment of high-frequency plasma insulin oscillations in control and type 2 diabetic subjects. *Diabetes.* 48:714–721.
31. Pørksen, N., C. Juhl, …, O. Schmitz. 2000. Concordant induction of rapid in vivo pulsatile insulin secretion by recurrent punctuated glucose infusions. *Am. J. Physiol.* 278:E162–E170.
32. Huard, B., A. Bridgewater, and M. Angelova. 2017. Mathematical investigation of diabetically impaired ultradian oscillations in the glucose-insulin regulation. *J. Theor. Biol.* 418:66–76.
33. Li, J., Y. Kuang, and C. C. Mason. 2006. Modeling the glucose-insulin regulatory system and ultradian insulin secretory oscillations with two explicit time delays. *J. Theor. Biol.* 242:722–735.
34. Sturis, J., K. S. Polonsky, …, E. Van Cauter. 1991. Computer model for mechanisms underlying ultradian oscillations of insulin and glucose. *Am. J. Physiol.* 260:E801–E809.
35. Bai, F., R. Bertram, and B. R. Karamched. 2022. A closed-loop multi-scale model for intrinsic frequency-dependent regulation of axonal growth. *Math. Biosci.* 344:108768.
36. Bertram, R., L. Satin, …, A. Sherman. 2004. Calcium and glycolysis mediate multiple bursting modes in pancreatic islets. *Biophys. J.* 87:3074–3087.
37. Simon, C., G. Brandenberger, …, M. Follenius. 1994. Slow oscillations of plasma glucose and insulin secretion rate are amplified during sleep in humans under continuous enteral nutrition. *Sleep.* 17:333–338.
38. Simon, C., M. Follenius, and G. Brandenberger. 1987. Postprandial oscillations of plasma glucose, insulin and C-peptide in man. *Diabetologia.* 30:769–773.
39. Simon, C., and G. Brandenberger. 2002. Ultradian oscillations of insulin secretion in humans. *Diabetes.* 51:S258–S261.
40. Levy, J. C. 2001. Insulin signalling through ultradian oscillations. *Growth Hormone IGF Res.* 11:S17–S23.
41. Simon, C. 1998. Ultradian pulsatility of plasma glucose and insulin secretion rate: circadian and sleep modulation. *Horm. Res.* 49:185–190.
42. Sturis, J., A. J. Scheen, …, E. van Cauter. 1995. 24-hour glucose profiles during continuous or oscillatory insulin infusion. Demonstration of the functional significance of ultradian insulin oscillations. *J. Clin. Invest.* 95:1464–1471.
43. Scheen, A. J., J. Sturis, …, E. Van Cauter. 1996. Alterations in the ultradian oscillations of insulin secretion and plasma glucose in aging. *Diabetologia.* 39:564–572.
44. O'Meara, N. M., J. Sturis, …, K. S. Polonsky. 1993. Lack of control by glucose of ultradian insulin secretory oscillations in impaired glucose tolerance and in non-insulin-dependent diabetes mellitus. *J. Clin. Invest.* 92:262–271.
45. Tolić, I. M., E. Mosekilde, and J. Sturis. 2000. Modeling the insulin-glucose feedback system: the significance of pulsatile insulin secretion. *J. Theor. Biol.* 207:361–375.
46. Pørksen, N., B. Nyholm, …, O. Schmitz. 1997. In humans at least 75% of insulin secretion arises from punctuated insulin secretory bursts. *Am. J. Physiol.* 273:E908–E914.
47. Pørksen, N., S. Munn, …, P. Butler. 1995. Pulsatile insulin secretion accounts for 70%of total insulin secretion during fasting. *Am. J. Physiol.* 269:E478–E588.
48. Meier, J. J., J. D. Veldhuis, and P. C. Butler. 2005. Pulsatile insulin secretion dictates systemic insulin delivery by regulating hepatic insulin extraction in humans. *Diabetes.* 54:1649–1656.
49. Sturis, J., K. S. Polonsky, …, E. van Cauter. 1992. Abnormalities in the ultradian oscillations of insulin secretion and glucose levels in type 2 (non-insulin-dependent) diabetic patients. *Diabetologia.* 35:681–689.